

High-order 3D FEM of Prostate Needle Insertion Forces

Anitha Priya Krishnan

Department of Biomedical Engineering
University of Rochester

601 Elmwood Avenue, Rochester, NY 14642
ankrishn@bme.rochester.edu

Walter G.O'Dell

Departments of Radiation Oncology and Biomedical Engineering
University of Rochester

601 Elmwood Avenue, Rochester, NY 14642
walter_odell@urmc.rochester.edu

Abstract—The long term goal of this project is to predict the deformation brachytherapy needle insertion using a 3D finite element model (FEM). Our FEM was based on a realistic prostate geometry obtained from ultrasound images from a human patient subject, including the geometry of the urethra and prostate capsule. The model was used to investigate pin cushion deformation that occurs during brachytherapy just prior to puncture of the capsule. A 2D FEM was used previously to validate the approach. The 2D FEM employed non-linear element basis functions and the model predictions were compared to those reported in the literature. The current study employed a 3D FEM model with code developed in Matlab and using linear combinations of cubic Hermite finite element basis functions. The material properties for the prostate were those obtained from the literature. The base mesh was defined as an ellipsoidal prostate and capsule, with 48 nodes defining the prostate surface. The urethra was modelled as a paraboloid running through the prostate. The nodal parameters of the prostate base mesh were then optimized to match the unique anatomy of the representative human prostate under investigation. The surface fitting error after optimization was 1.4mm. Finally, a 10N axial force was applied to an apical capsule node and the deformed mesh satisfying force balance equilibrium was converged to in approximately 1 hour. A 8% reduction was found for the overall axial displacement of the node at which the force was applied when the results using the encapsulated prostate model was compared to previous results where the capsule was not included. This finding suggests that the capsule plays a prominent mechanical role in brachytherapy needle insertion and warrants a more in-depth study of capsule mechanical properties.

Index Terms—Brachytherapy, Finite element method, cubic hermite basis functions, pin cushion deformation, prostate

I. INTRODUCTION

Brachytherapy is a form of radiation therapy in which radioactive sources are placed in direct contact with the tissue to be treated. Prostate cancer is currently the second leading cause of cancer death among men [1]. Some of the methods used to treat prostate cancer are radical prostatectomy (surgical removal of the entire prostate and seminal vesicles), radiation therapy, hormonal therapy and chemotherapy. The advantage of brachytherapy is that it can deliver more radiation to the prostate with lower dose to the surrounding normal organs than conventional external beam radiation therapy and has associated with it a shorter recovery time. This higher intraprostatic dose should theoretically result in more effective tumor sterilization [2].

Inserting and retracting the needles during seed deposition causes the surrounding tissues to deform. Ignoring these deformations results in misplaced seeds and poses a problem in avoiding vital organs. Although real time ultrasound imaging is available during the procedure, it often does not produce crisp tissue boundaries at all time points. In addition, 2D ultrasound imaging cannot effectively track the penetration of the needle into the deformed prostate because the needle can follow an oblique trajectory that leaves the 2D imaging plane. A model developed to predict deformation of the prostate tissue explicitly would be helpful in automating the surgery and thereby reducing placement errors and improving treatment outcome.

Simulations of needle insertion for training purposes have been implemented previously using FEM. A simulation environment for measuring planar tissue deformation during needle insertion was developed by DiMaio and Salcudean [3], [4]. Force measurements of needle insertion of a soft tissue phantom were obtained using a robotic manipulator and displacements were measured using a CCD camera to record the needle insertion procedure. The measured deformation was then compared with the deformation from FEM simulation and the friction forces along the needle shaft were estimated. An interactive 2D simulation was developed using a linear elastic tissue model and the same friction profile to model the interaction between the needle and the tissue.

Alterovitz *et al.* [5], [6] developed a 2D simulation of needle insertion and seed deposition using a linear elastic FEM for training and planning for prostate brachytherapy. The effect of tissue properties and needle characteristics on accuracy of seed placement was predicted by varying tissue and friction parameters in the model.

The above mentioned methods cannot be readily generalized to 3D as this would substantially increase the problem size requiring many elements and thereby increasing the computation cost. To overcome this problem Nienhuys *et al.* [7] proposed a computational technique based on iterative algorithms that do not require pre-computed structures. Their 3D model used 30,000 elements which is an increase by a factor of 47 over the number of elements used in their 2D model. Since the 3D matrix operations are 2 to 3 times more expensive, the computational cost of a 3D simulation was larger by a factor of 120.

In each of the above stated methods the images both before and after deformation were available and the de-

formation of the organ or phantom was calculated by the finite element model so that it resembled the deformation seen in the deformed image. For the case of prostate brachytherapy however, there is a need to account for the deformation before it occurs. Also, in these former approaches the force distribution was obtained from the deformation pattern whereas what is needed is a model that predicts the deformation pattern given the force profile. The current work aims to overcome these limitations.

The finite element models used by the previous authors are based on 2D linear elements and when extended to 3D these require many elements to faithfully reproduce the underlying geometry. This demands an increased computation cost. We propose to overcome this drawback by using nonlinear elements which use fewer nodes and elements to reproduce the geometry and therefore less storage space and computational time.

II. METHODS

A. FEM software

Finite element analysis is useful for interpolating tissue geometries between reference and deformed states. During a needle insertion procedure, a needle is inserted into the prostate after first penetrating the perineum and the intervening tissue before reaching the apex of the prostate. The forces necessary to puncture these outer surface membranes and then to continue penetrating through the prostate zonal anatomy produce a pin cushion deformation at the site of needle insertion.

The finite element model implemented here uses higher order spatial interpolation within each element that assures a continuous and smooth deformation field within and across elements. This method of interpolation achieves a more realistic representation of large tissue deformations than linear spatial interpolation. The analysis code was written in MATLAB and incorporates many features unique to modelling large deformations, non-linear spatial interpolation within elements and smoothly continuous deformation across elements. Our FEM formalism also does not require material incompressibility, as is often required by commercial finite element packages.

B. Anatomical model of the prostate

A 3D anatomical model of the prostate was reconstructed from serial ultrasound images obtained in a human subject undergoing prostate brachytherapy for treatment of prostate cancer. From these surface measurements a cubic Hermite finite element model was generated to reconstruct the 3D prostate anatomy, including the urethra passing through the prostate. The prostate mechanical behavior was modelled using a linear elastic, incompressible and isotropic material model [8].

The base mesh for the prostate was an ellipsoid and the urethra was modelled as a tube whose long axis followed a parabolic trajectory through the prostate and terminating at the bladder at the antero-superior aspect of the prostate. The prostate capsule was modelled as a

2mm thick shell that encapsulated the prostate. This base mesh geometry was first aligned with the contour point dataset extracted manually from the ultrasound images. The nodes of the prostate mesh were then allowed to displace until an optimal match of the prostate mesh surface to the contour point array was obtained. The surface optimization routine utilized the MatLab optimization toolbox and was terminated when the fitting error fell within a prescribed error threshold; where the fitting error was defined as the mean-squared miss distance between measured 3D surface point locations and the closest FEM surface at each point.

C. Boundary conditions

The *in-vivo* prostate is constrained mechanically by the urethra and the surrounding bladder, rectum, seminal vesicles, the puboprostatic ligaments attached to the pubic bone, the superior fascia of the urogenital diaphragm and by portions of the Levatores ani muscle group. During brachytherapy the needle imposes a force on the prostate that is directed primarily in the inferior-superior direction. The bladder provides the primary boundary constraint at the prostate basal end. Therefore, to simplify the analysis we assume the bladder and urethra effects dominate. During the implantation procedure the prostate experiences two types of mechanical reaction to the forces imparted by the insertion needle: rigid body motion and deformation. After the prostate impinges on the bladder there is a reactive force from the bladder which restricts the rigid body motion and consequently the prostate undergoes deformation from this point. In this study we are interested primarily in the deformation of the prostate after rigid body motion has occurred and thus the effect of bladder is simulated by fixing the displacement of nodes of the prostate capsule at the basal end around the opening of the urethra.

The urethra was made stiffer than the prostate to simulate the foley catheter that is inserted into it during surgery to stabilize the prostate. The material properties of each anatomical component are characterized by their Young's modulus and Poisson's ratio. A Young's modulus five times the value of the one used for prostate was used to model urethra. To depict the role of the capsule on the overall prostate mechanics during needle insertion, two separate FEM simulations were computed with the first using a stiffness for the capsule of thrice that of the prostate. The second run then used the same parameters for both the prostate and the capsule, effectively eliminating the capsule.

D. Finite Element Method

The displacements and geometry were interpolated using cubic Hermite basis functions, as taken from [9], which provide continuity of the derivatives across element boundaries. The one dimensional cubic Hermite basis functions are as follows:

$$\Psi_1^0(\xi) = 1 - 3\xi^2 + 2\xi^3 \quad (1)$$

$$\Psi_1^1(\xi) = \xi(\xi - 1)^2 \quad (2)$$

$$\Psi_2^0(\xi) = \xi^2(3 - 2\xi) \quad (3)$$

$$\Psi_2^1(\xi) = \xi^2(\xi - 1) \quad (4)$$

The bi-cubic Hermite basis functions were used to depict the curvilinear surfaces in 2D. Each node in 2D has the following parameters.

$$x, \frac{\partial x}{\partial s_1}, \frac{\partial x}{\partial s_2}, \frac{\partial^2 x}{\partial s_1 \partial s_2}, y, \frac{\partial y}{\partial s_1}, \frac{\partial y}{\partial s_2}, \frac{\partial^2 y}{\partial s_1 \partial s_2}, z, \frac{\partial z}{\partial s_1}, \frac{\partial z}{\partial s_2}, \frac{\partial^2 z}{\partial s_1 \partial s_2}$$

The bi-cubic interpolation of the nodal parameters is given by

$$\begin{aligned} u(\xi_1, \xi_2) = & \Psi_1^0(\xi_1)\Psi_1^0(\xi_2)u_1 + \Psi_2^0(\xi_1)\Psi_1^0(\xi_2)u_2 \\ & + \Psi_1^0(\xi_1)\Psi_2^0(\xi_2)u_3 + \Psi_2^0(\xi_1)\Psi_2^0(\xi_2)u_4 \\ & + \Psi_1^1(\xi_1)\Psi_1^0(\xi_2) \left(\frac{\partial u}{\partial \xi_1} \right)_1 \\ & + \Psi_2^1(\xi_1)\Psi_1^0(\xi_2) \left(\frac{\partial u}{\partial \xi_1} \right)_2 \\ & + \Psi_1^1(\xi_1)\Psi_2^0(\xi_2) \left(\frac{\partial u}{\partial \xi_1} \right)_3 \\ & + \Psi_2^1(\xi_1)\Psi_2^0(\xi_2) \left(\frac{\partial u}{\partial \xi_1} \right)_4 \\ & + \Psi_1^0(\xi_1)\Psi_1^1(\xi_2) \left(\frac{\partial u}{\partial \xi_2} \right)_1 \\ & + \Psi_2^0(\xi_1)\Psi_1^1(\xi_2) \left(\frac{\partial u}{\partial \xi_2} \right)_2 \\ & + \Psi_1^0(\xi_1)\Psi_2^1(\xi_2) \left(\frac{\partial u}{\partial \xi_2} \right)_3 \\ & + \Psi_2^0(\xi_1)\Psi_2^1(\xi_2) \left(\frac{\partial u}{\partial \xi_2} \right)_4 \\ & + \Psi_1^1(\xi_1)\Psi_1^1(\xi_2) \left(\frac{\partial^2 u}{\partial \xi_1 \partial \xi_2} \right)_1 \\ & + \Psi_2^1(\xi_1)\Psi_1^1(\xi_2) \left(\frac{\partial^2 u}{\partial \xi_1 \partial \xi_2} \right)_2 \\ & + \Psi_1^1(\xi_1)\Psi_2^1(\xi_2) \left(\frac{\partial^2 u}{\partial \xi_1 \partial \xi_2} \right)_3 \\ & + \Psi_2^1(\xi_1)\Psi_2^1(\xi_2) \left(\frac{\partial^2 u}{\partial \xi_1 \partial \xi_2} \right)_4 \end{aligned} \quad (5)$$

In 3D each node has eight parameters per coordinate direction and hence 24 parameters per node. The finite element solution was based on Galerkin weighted residual formulation. A force due to needle insertion was applied to one node at the apex of the prostate and near the opening for the urethra. The force was directed superiorly. The stress at every node in the mesh was calculated by integrating the displacement field at the Gauss points;

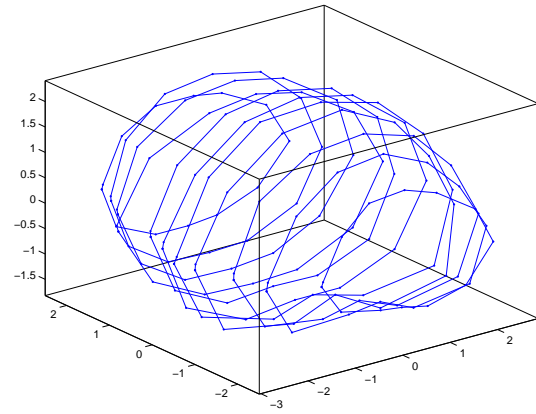


Fig. 1. The contour points obtained from ultrasound images representing geometry of the different slices

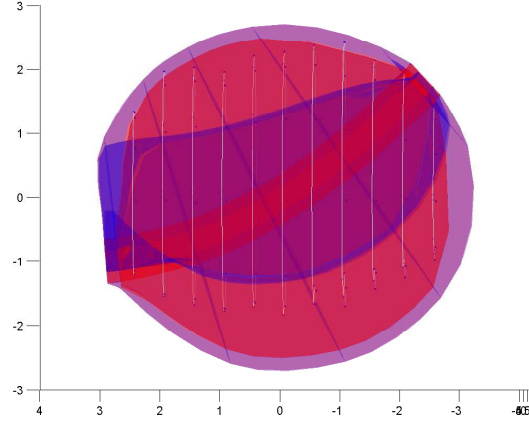


Fig. 2. The initial mesh before optimization. The white contours represent the contour points from ultrasound.

computing the 3D strain tensor in the neighborhood of each point, and using the material model to estimate the second Piola-Kirchhoff stress at each Gauss point. After computing the associated Cauchy stress tensor, the residual stress field was computed. From this residual the nodal parameters were adjusted until the following Galerkin-weighted force balance equation was satisfied.

$$\iiint \left(\frac{dT_x x}{dx} + \frac{dT_x y}{dy} + \frac{dT_x z}{dz} \right) \cdot \omega_i dx dy dz = 0 \quad (6)$$

where T represents the stress and ω represents the weight for elemental basis function i .

The above equation is the force balance equation along the 'x' direction. There is one such equation for each weighting function i . The 3D FEM consisted of a combined 156 nodes and 96 elements for the prostate, urethra and capsule.

III. RESULTS

A. Mesh Initialization

A 2D FE mesh was created for each ultrasound image slice. For this subject the slices were acquired at 5 mm

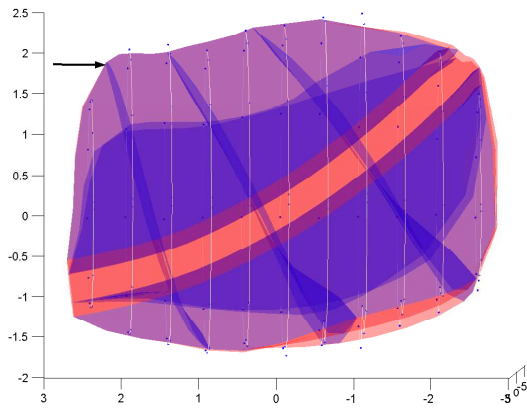


Fig. 3. The 3D mesh fitted to ultrasound data points. The arrow represents the direction and point of application of force.

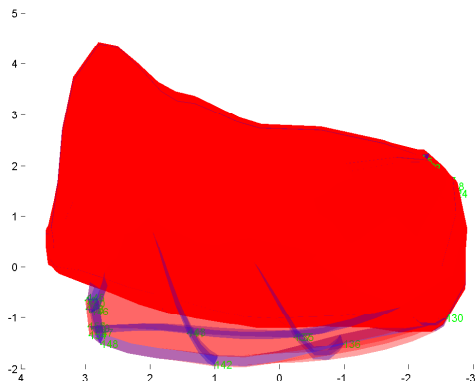


Fig. 4. The deformed mesh after applying a force of 10N. The capsule has the same stiffness as the prostate.

increments across the organ and 11 image slices were needed to span the entire prostate. The prostate border was manually contoured and there were generated between 19 and 40 contour points for each slice. The complete contour point dataset obtained from the ultrasound images is shown in Figure 1. Optimization for a typical 2D slice required less than a minute of computation time and achieved an average a fitting error of 1.7 mm. The 2D mesh models were used to generate a more uniformly sampled 3D set of 88 prostate contour points. The base 3D mesh before surface fitting is shown in Figure 2. The fitted mesh is shown in Figure 3. The fitting of 3D mesh nodal parameters to the 88 uniformly sampled contour points took approximately 15 minutes and achieved a fitting error of 1.42 mm.

B. Mesh Deformation

A concentrated force of 10N was applied at a central inferior node of the capsule, while fixing some of the nodes at the superior end to avoid rigid body translation of the entire organ. The displacement at the point of load was calculated. *In-vivo* needle insertion force measurements conducted at

our institution established that 10N is a typical maximal needle insertion during prostate brachytherapy [10], [11]. In the model where the capsule was given the same stiffness as the prostate parenchyma, the node at the site of loading experienced an overall displacement of 2.61 cm. In the model where the capsule stiffness was 3x larger than that of the prostate parenchyma the displacement at the site of loading was 2.46 cm. The deformed mesh when the capsule had the same stiffness as the prostate parenchyma is shown in Figure 4. The optimization over 3500 nodal degrees of freedom took approximately one hour to converge on a 2.6 GHz Windows based PC running Matlab 6.1 with the optimization toolbox.

IV. DISCUSSION

In this paper we have presented a novel 3D FEM of the prostate to predict deformation of the prostate during brachytherapy needle insertion. The prostate is modelled as a linear elastic material in the current FEM. The inclusion of the capsule in the model changed the dynamics of needle insertion. A force of 10N produced a displacement of 2.46 cm. This was less than the displacement observed when the capsule had the same stiffness as the prostate (2.61 cm). However, *in-vivo* experiments conducted at our institution indicate that once the needle penetrated the capsule comparatively less force is experienced [10], [11]. The initial results emphasize the importance of capsule in the dynamics of needle insertion prior to needle penetration into the prostate parenchyma, suggesting that a more in depth analysis of the capsule material properties should be undertaken. Our next goal is to conduct *in-vivo* needle insertion experiments to obtain more realistic values for material properties of prostate.

Our method of restraining a few nodes at the superior end of the prostate did not reproduce well the boundary conditions offered by the bladder, thereby a non-negligible rotation was observed in the prostate. In the future the FEM will be improved by including a mesh for the bladder to provide a more realistic boundary condition, including large strain analysis and modelling the prostate as visco-elastic material. Finally, the effect of the presence of tumors on the deformation will be simulated by creating a localized region of increased stiffness within the prostate.

ACKNOWLEDGMENT

This research was supported by NIH/NIC grant R01 CA091763 and the American Cancer Society RSG-02-155-01-CCE.

REFERENCES

- [1] Wingo, P., Tong, T., Bolden, S.: Cancer statistics. *CA Cancer J Clin* **45** (1995) 8–30
- [2] Porter, A.T., Blasko, J., Grimm, P., Reddy, S., H.Ragde: Brachytherapy for prostate cancer. *CA Cancer J Clin* **45** (1995) 165–178
- [3] DiMaio, S.P., Salcudean, S.: Needle insertion modeling and simulation. *IEEE transactions on Robotics and Automation* **19** (2003) 864–875
- [4] DiMaio, S.P., Salcudean, S.: Needle insertion modeling for the interactive simulation of percutaneous procedures. In: *Proceedings of Medical image computing and computer-assisted intervention (MICCAI'02)*. (2002) 253–260

- [5] Alterovitz, R., Pouliot, J., Taschereau, R., Hsu, I.C.J., Goldberg, K.: Simulating needle insertion and radioactive seed implantation for prostate brachytherapy. In J.D. Westwood et al., editor, *Medicine meets virtual reality 11 (MMVR11)* (2003) 19–25
- [6] Alterovitz, R., Pouliot, J., Taschereau, R., Hsu, I.C.J., Goldberg, K.: Needle insertion and radioactive seed implantation in human tissues: Simulation and sensitivity analysis. In: *Proceedings of 2003 IEEE international conference on Robotics and Automation (ICRA 2003)*. Volume 2. (2004) 1793 – 1799
- [7] Nienhuys, H., van der Stappen, A.: A computational technique for interactive needle insertions in 3d nonlinear material. In: *Proceedings of 2004 IEEE international conference on Robotics and Automation (ICRA 2004)*. (2004) 2061–2067
- [8] Krouskop, T., Wheeler, T., Kallel, F., et al: Elastic moduli of breast and proatate tissues under compression. *Ultrasonic Imaging -* (1998) 260–274
- [9] Hunter, P. J, Pullan, A. J: FEM/BEM Notes, Available on the WWW via <http://www.bioeng.auckland.ac.nz/cmiss/fembemnotes/fembemnotes.pdf>
- [10] T.K. Podder, D.P. Clark, D. Fuller, E.M. Messing, D.J. Rubens, J.G. Strang, J. Sherman, R.A. Brasacchio, and Y. Yu: In Vivo Force-Torque Measurement during Prostate Brachytherapy. In: 47th Annual Meeting of the American Association of Physicists in Medicine. 2005 (SU-FF-T-204)
- [11] T.K. Podder, E.M. Messing, D.J. Rubens, J.G. Strang, D.P. Clark, D. Fuller, J. Sherman, R.A. Brasacchio, W.S. Ng, and Y. Yu Brachytherapy Needle Insertion: an in Vivo Data Analysis In: *International Conference of Medical Physics (ICMP-2005,580)*
- [12] A Krishnan, Y Yu, W O'Dell 3D FEM of the Prostate to Predict Deformation During Brachytherapy Needle Insertion In: 46th Annual Meeting of the American Association of Physicists in Medicine. 2004 (SU-GG-PDS-15)